Integrating building energy simulation with a machine learning algorithm for evaluating indoor living walls' impacts on cooling energy use in commercial buildings

Liping Wang [a]*, Michael J. Witte [b]

[a] Civil and Architectural Engineering, University of Wyoming, 1000 E University Ave., Laramie, WY, 82071

[b] GARD Analytics Inc., 1334 N Walnut Ave., Arlington Heights, IL 60004

Abstract

The environmental challenges of climate change increase the energy usage and peak demands of buildings. Most extant studies of greenery systems focus on exterior applications such as green façades and roofs, which indirectly affect the indoor environment. Few studies have focused on quantifying the influence of indoor greenery systems on building energy consumption. The cooling effects of indoor greenery systems such as living walls are largely accounted for by the evapotranspiration (ET) process, in which water is transferred to the ambient environment through the evaporation from and transpiration of plants. Current building energy simulation software such as EnergyPlus did not have a module for modeling indoor greenery systems.

In this study, an ET model was created using a machine learning algorithm—Gaussian Mixture Regression (GMR) based on experimental data. An indoor living wall model quantifying sensible and latent loads from the ET process was integrated with the energy simulation software—EnergyPlus through the Python plugin feature. The U.S. Department of Energy (DOE) medium-sized office building reference model was modified and used in this study to evaluate indoor living walls' impacts on cooling energy use. A parametric study on leaf to floor area ratios (LFAR), orientations, distances from windows, and climates was conducted to evaluate the influence of each factor on indoor living walls' performance. Cooling effects of indoor living walls were evaluated in three ASHRAE climates with high cooling demands. Observable cooling energy savings were obtained for the south, east, and west perimeter zones while savings for the north perimeter zone was negligible in all three climates. With the consideration of extra electricity use from direct expansion (DX) dehumidification devices for humidity control, the maximum cooling electricity savings in Los Angeles, CA are 25.1% when LFAR=1.5 for the south perimeter zone, 14.4% when LFAR=0.5 for the east perimeter zone, 0.3% when LFAR=0.3 for the north perimeter zone, and 14.5% when LFAR=0.5 for the west perimeter zone on the design day.

Keywords: indoor living walls; evapotranspiration; machine learning; EnergyPlus; Python

1. Introduction

The environmental challenges of climate change further increase the energy usage and peak demands of buildings. Various efforts have been made to reduce building energy

consumption while maintaining a comfortable indoor environment. Greenery infrastructure enhancements have been recognized as climate change adaptation measures by the Intergovernmental Panel on Climate Change (IPCC) [1, 2], and have been considered effective approaches for addressing climate challenges through mitigation of the urban heat island effect [3-5], passive cooling [6, 7], and air quality improvement [8, 9]. The cooling effects of greenery systems are largely accounted for by the evapotranspiration (ET) process, in which water is transferred to the ambient environment through the evaporation from and transpiration of plants [10].

Most extant studies of greenery systems focus on exterior applications such as green façades and roofs, which indirectly affect the indoor environment. Limited studies have been conducted on indoor greenery systems such as indoor living walls despite the fact that people on average spend about 90% of their time indoors [11]. Few studies have focused on quantifying the influence of indoor greenery systems on building energy consumption. Previous work on indoor greenery systems has only demonstrated proof-of-concept results on cooling effect [12-14], and has not attempted to quantify how different sizes of indoor greenery systems affect building energy consumption. In an experimental study of a hall with a floor area of 520 ft^2 that was not equipped with air conditioning, an average temperature reduction of 4K was observed near an 86 ft^2 indoor living wall [12]. Perez-Urrestarazu et al. [13] performed an experiment using an active living wall in the hallway of a faculty building in Seville, Spain. The hallway was not supplied by the building's HVAC system. Results showed drops in temperature between 0.8 and 4.8K at different distances from the wall due to the presence of the living wall. Thus, an indoor greenery system can potentially be an alternative to a mechanical evaporative cooler for space cooling. Abdo and Huynh [14] tested living walls within rectangular acrylic-sheets chambers (0.5m×0.5m×0.13m) in Sydney, Australia. Experimental results showed that living walls reduced the ambient temperatures in a range of 0.5–3K depending on whether a living wall is in an active (with a mechanical fan) or passive (without mechanical ventilation) chamber environment. In addition, indoor plants demonstrate the capability of improving thermal comfort [15], indoor air quality [16-20], productivity and creativity [21, 22], while reducing noise levels [23], the negative effects of visual glare [24], stresses [25, 26], and discomforts [27, 28]. The diverse ecosystem created by indoor greenery systems opens up new opportunities for counteracting climate change through integration with heating, ventilation, and air conditioning (HVAC) systems in commercial buildings.

Because the cooling effects of indoor living walls are largely accounted for by the evapotranspiration (ET) process, accurately determining the ET rates is essential for the quantification of indoor living walls' impacts on HVAC energy use. ET rates are affected by environmental conditions (air temperature, humidity, air velocity, net radiation) [29], plant type [30], plant physiology parameters (leaf area index, leaf temperature, plant density [31]), and plant growing methods (soil-based or hydroponics). Although approximately fifty ET models [32-47] have been developed and widely applied for open-field agriculture, forests, and wetlands, only a couple of ET models (Stanghellini and Graamans's models) were created for controlled environment agriculture [29]. A few studies [48-50] have employed existing ET models such as Penman-Monteith [32] and FAO Penman-Monteith [51] for ET prediction of outdoor greenery systems. But no studies have conducted ET modeling for indoor greenery systems in buildings.

The objectives of this study are 1) to create a thermal model for indoor greenery systems to predict ET rates and thermal interaction with the indoor environment, and 2) to evaluate the impacts of indoor living walls on HVAC energy consumption using the DOE medium-sized office building prototype [53]. In this study, plant experiments using a portable photosynthesis system LI-6400XT were first presented in section 2 to measure transpiration and stomatal conductance of hydroponically growing indoor plants at various environmental conditions. Section 3 describes the ET and stomatal conductance models built upon measurement data from plant experiments. Particularly, a Gaussian mixture regression (GMR) model was developed for modeling ET of indoor hydroponic greenery systems. Section 4 describes the method of modeling indoor living walls built upon the GMR model for quantification of ET rates. An indoor living wall model quantifying sensible and latent loads from the ET process was integrated with the energy simulation software—EnergyPlus [52] through the Python plugin feature. Sections 5 and 6 present the parametric simulation study using coupled simulations between the indoor living wall model and EnergyPlus and simulation results. Energy simulations were carried out for summer design days in three climates. Preliminary design guidelines on indoor living walls were put forward for architects and mechanical engineers.

2. Plant experiments

The portable photosynthesis system LI-6400XT [54] was used to measure transpiration and stomatal conductance of hydroponically growing indoor plants. LI-6400XT is commonly used to compute leaf-level photosynthesis based on the measured difference in CO_2 and H_2O between controlled environmental chamber conditions and reference conditions [54]. LI-6400XT was able to set up different leaf chamber environmental conditions (temperature, humidity, CO_2, and net radiation) and measure plants' physiological responses to various environmental conditions. Stomatal conductance [mmol m^{-2} s^{-1} or m/s] represents the degree of stomatal openings and directly affects the rate of water vapor exiting through stomata [55].

Figure 1. The leaf chamber sensor head, LI-6400XT for plant physiological measurements

Specifically, a common type of indoor plant—*Epipremnum aureum (Golden Pothos)*—was selected. As shown in Figure 1, *Epipremnum aureum* was planted in a hydroponic growing system that was made from PVC pipes (pipe diameter: 2.5 inches) partially filled with the nutrient solution.

The experiments were designed and carried out for different chamber environmental conditions. These environmental parameters include photosynthetic photon flux density (PPFD), CO_2 concentration, and chamber block temperature. Plants make use of the light region between 400 nm and 700 nm referred to as photosynthetically active radiation (PAR) for photosynthesis.

PPFD [µmol/s-m^2] measures the amount of photosynthetically active photons (400 nm-700 nm) arriving at a leaf surface per m^2 per second.

Five plants were randomly selected and labeled from the hydroponic system. The sensor head of LI-6400XT is shown in Figure 1. The PPFD levels were tested at 10, 50, 100, 200, 300, 400, 500, 600, 700, 800, 900, and 1000 µmol/s-m^2. The CO_2 concentration levels were tested at 300-1500 ppm with 100 ppm intervals. The chamber block temperatures were set at 18-35 ºC with 1ºC intervals.

Each measurement in response to the change of lighting or temperature was taken after waiting for at least 30 minutes from the change of chamber lighting conditions and block temperature, or stabilization of the photosynthesis and stomatal conductance, whichever is longer. Each measurement in response to the change of CO_2 concentration was taken after a couple of minutes from the change of chamber CO_2 concentrations or stabilization of the photosynthesis and stomatal conductance, whichever is longer. "Match" is always applied to trigger the operation of the match valve of LI-6400XT every 20-30 minutes or after the change of CO_2 concentrations in the leaf chamber.

Based on the experimental data, the relationships between key environmental parameters and transpiration rates as well as stomatal conductance of the indoor plants were illustrated in Figures 2-5. PPFDs have the most significant impact on plants' stomatal conductance and transpiration in comparison with CO_2 concentrations and the chamber block temperature. Figure 2 shows that transpiration rates increased with the increase of PPFD until it reached 700 µmol/(s-m^2) and plateaued. Transpiration rates ranged from 0 mmol H_2O/(m^2s) to 1.95 mmol H_2O/(m^2s) with the variation of PPFDs under the testing condition of block temperature: 20 ºC, CO_2 concentration: 400 ppm, and relative humidity: 40%-70%.

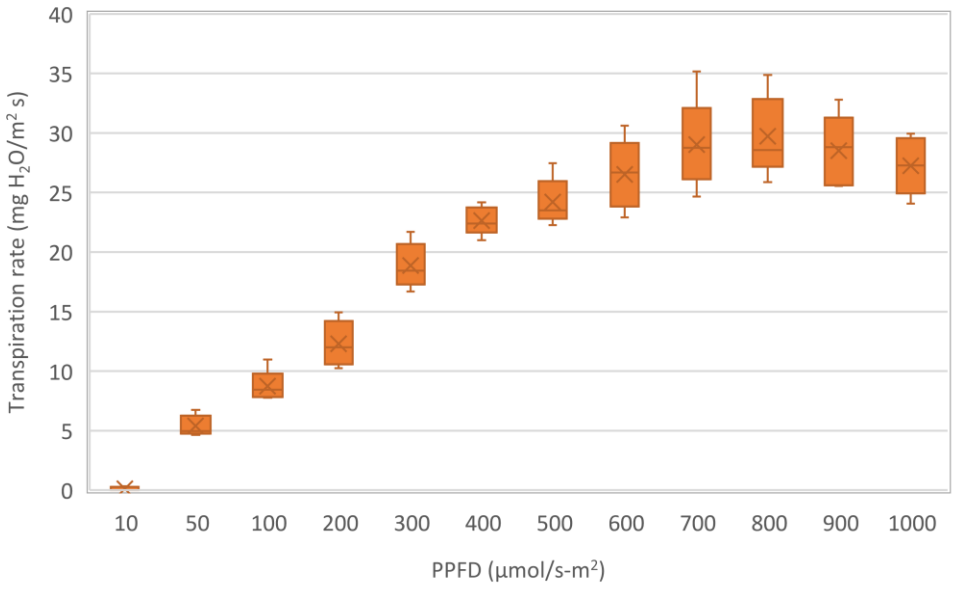

Figure 2. Transpiration rates of *Epipremnum aureum* in response to different photosynthetic photon flux density (PPFD) under the testing condition of block temperature: 20 ºC, CO_2 concentration: 400 ppm, and relative humidity: 40%-70%

Figures 3 showed changes in transpiration in response to the increase in CO_2 concentrations. Transpiration rates stayed nearly constant when CO_2 concentration ranges from 300 ppm to 500 ppm under the testing condition of block temperature: 20 ºC, PPFD: 100 µmol/(s-m^2), and relative humidity: 40%-70%. However, with the further increase of CO_2 concentrations, transpiration rates decreased because plant stomata tend to close with largely increased CO_2 concentrations. The medians of stomatal conductance and transpiration dropped by 56% and 54% respectively when CO_2 concentrations were continuously increased from 500 ppm to 1500 ppm.

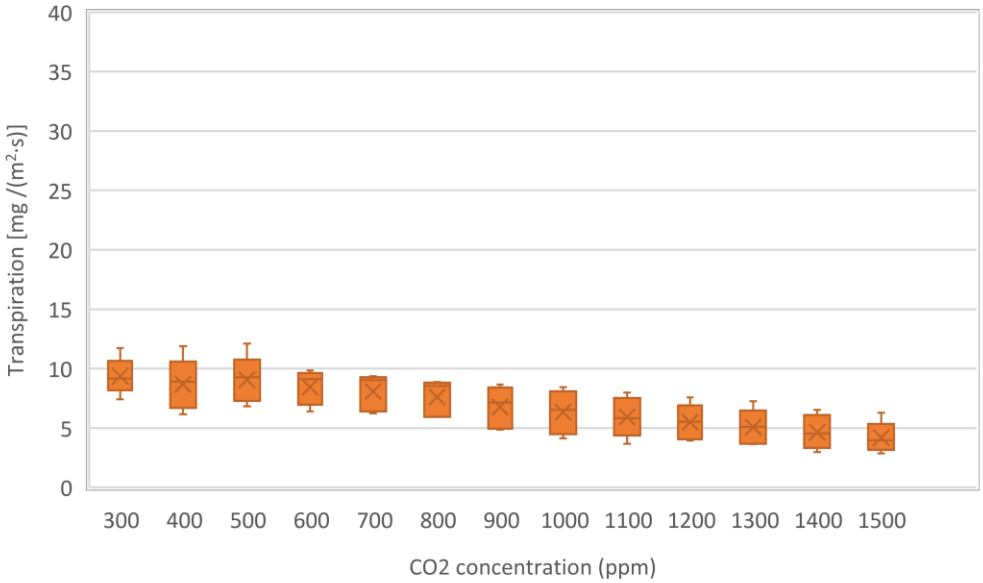

Figure 3. Transpiration rates of *Epipremnum aureum* in response to different CO_2 concentrations under the testing condition of block temperature: 20 ºC, PPFD: 100µmol/(s-m^2), and relative humidity: 40%-70%.

In addition to the variations of PPFD and CO_2 concentrations of testing environmental conditions, the chamber block temperatures were modified to evaluate the effect of block temperature on transpiration rates and stomatal conductance. As shown in Figure 4, transpiration rates of *Epipremnum aureum* increased with the increase of chamber block temperature from 18 ºC to 23 ºC. Transpiration rates plateaued with the further increase of block temperature.

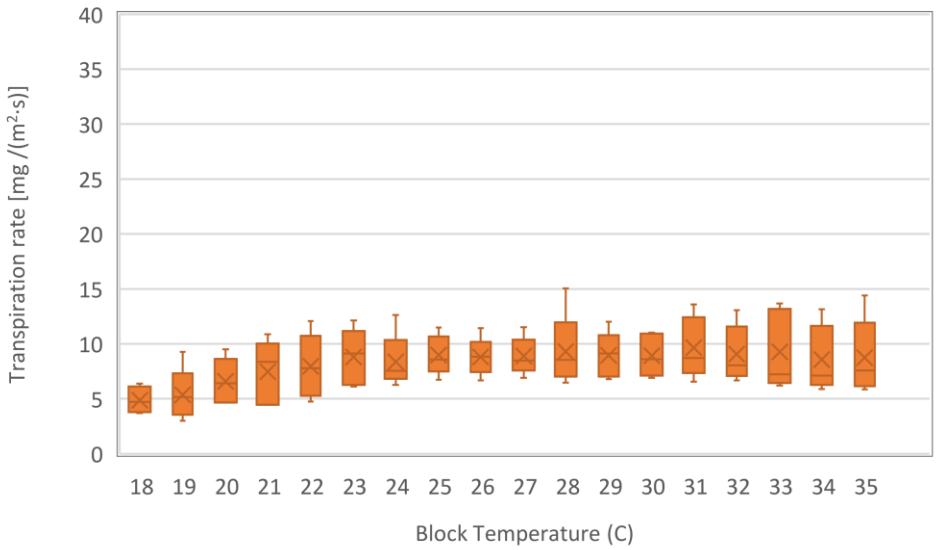

Figure 4. Transpiration rates of *Epipremnum aureum* in response to different block temperatures under the testing condition of CO_2 concentration: 400 ppm, PPFD: 100µmol/(s-m^2), and relative humidity: 40%-70%.

Stomatal conductance in response to the variation of block temperature is shown in Figure 5. Stomatal conductance slightly increased with the increase of block temperature of the chamber from 18 ºC to 23 ºC and stayed relatively steady between 24 ºC and 27 ºC. However, unlike transpiration rates, stomatal conductance decreased with the further increase of block temperature above 27 ºC. The median variation is up to 41% under the testing condition of CO_2 concentration: 400 ppm, PPFD: 100 µmol/(s-m^2), and relative humidity: 40%-70%.

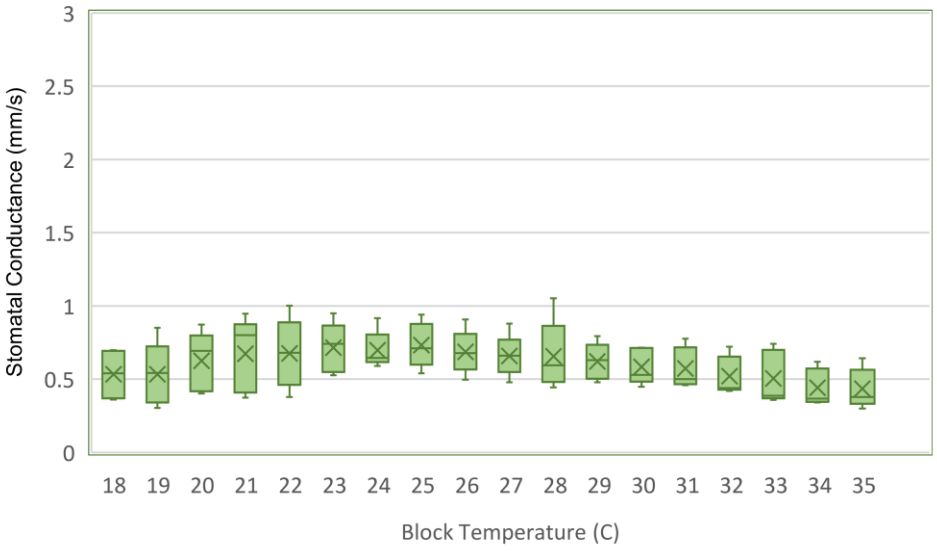

Figure 5. Stomatal conductance of *Epipremnum aureum* in response to different block temperatures under the testing condition of CO_2 concentration: 400 ppm, PPFD: 100 µmol/(s-m^2), and relative humidity: 40%-70%.

3. An ET model for indoor living walls

The measured ET and stomatal conductance tested under various chamber environmental conditions were used for training and/or testing three ET models: the Penman-Monteith model, a mass transfer ET model, and a GMR model for *Epipremnum aureum*. The evaporation from growing media of indoor living walls was neglected in this study. This is a reasonable assumption since the overall area of growing media is rather small for a hydroponic system.

3.1 ET models

3.1.1 *Penman-Monteith Model*

The Penman-Monteith model [32] (Eq. 1) has been widely used for ET prediction in agriculture [29] and was first tested using the experimental data for ET prediction of *Epipremnum aureum*.

$$ET = \frac{1}{\lambda}\frac{\Delta(I_n - G) + \frac{\rho_a \cdot Cp \cdot VPD}{r_a}}{\Delta + \gamma\left(1 + \frac{r_s}{r_a}\right)} \quad (1)$$

Where ET is the plant evapotranspiration rate [mm/s; kg/(m^{2}s)], λ is latent heat of vaporization [MJ/kg], Δ represents the slope of the saturation vapor pressure-temperature curve [kPa/°C], γ is the psychrometric constant [kPa/°C], I_n is the net radiation [MJ/m^2 s], G represents soil heat flux [MJ/m^2 s], ρ_a is mean air density [kg/m^3], Cp is the specific heat of air [MJ/kg °C], VPD is the vapor pressure deficit [kPa], r_s is (bulk) surface resistance [s/m] that describes the resistance to the flow of water vapor from inside the leaf, vegetation canopy, or soil to outside the surface, and r_a is aerodynamic resistance [s/m].

3.1.2 *Mass Transfer ET model*

In addition to the Penman-Monteith model, ET prediction based on a mass transfer equation (Eq. 2) based on the humidity ratio difference was also tested in this study.

$$ET = \frac{\rho_a A(W_p - W_a)}{(r_a + r_s)} \quad (2)$$

where ρ_a is mean air density [kg/m^3], A is the leaf area [m^2], W_a is humidity ratio [kg vapor/kg dry air], W_p is humidity ratio [kg vapor/kg dry air] of saturated air at plant surface temperature T_P, r_a is aerodynamic resistance [s/m], r_s is the stomatal resistance [s/m].

3.1.3 *Gaussian Mixture Regression (GMR) model*

A GMR model was used to predict ET rates for indoor plants using experimental data as the third ET model for comparison. GMR models have been tested in predicting energy use [58, 59] in the built environment as well as in other disciplines[60, 61]. Gaussian Mixture Model (GMM) is a parametric probability density function represented as a weighted sum of Gaussian component densities (Eq.3).

$$prob(\boldsymbol{x}) = \sum_{j=1}^{k} \pi_j N(\boldsymbol{x}, \boldsymbol{y} | \boldsymbol{\mu_j}, \delta_j) \quad (3)$$

Where π_j, $\boldsymbol{\mu_j}$, and δ_j denote the weight coefficient, mean, and covariance of the j^{th} component, respectively. $N(\boldsymbol{x}, \boldsymbol{y} | \boldsymbol{\mu_j}, \delta_j)$ represent the probability distribution function of a multi-variable

Gaussian process. The GMM parameters were determined using the Expected Maximization (EM) algorithm with training data. The optimal number of components can be determined based on the Bayesian Information Criterion [62] or the Variational Bayesian method [63]. GMR [64] is then used to predict the dependent variable $\hat{\boldsymbol{f}}(\boldsymbol{x})$ ET rates given the observed independent variables $\boldsymbol{x}$, such as net radiation (R_n), air temperature (T_a), CO_2 concentration C_a, and vapor pressure deficit (VPD), and GMM parameters for testing data. $\hat{\boldsymbol{f}}(\boldsymbol{x})$ represents the prediction of the dependent variable $\boldsymbol{f}(\boldsymbol{x})$. $w_j(\boldsymbol{x})$ is the updated mixing coefficient vector given observed independent variables for the j^{th} componentx.

$$\hat{\boldsymbol{f}}_k(\boldsymbol{x}) = E(Y|X=\boldsymbol{x}) = \sum_{j=1}^{k} w_j(\boldsymbol{x})\left(\mu_{jY} + \delta_{jYX}\delta_{jXX}{}^{-1}\left(\boldsymbol{x}-\boldsymbol{\mu_{jX}}\right)\right) \quad (4)$$

$$w_j(\boldsymbol{x}) = \frac{\pi_j N(\boldsymbol{x};\boldsymbol{\mu_{jX}},\delta_{jXX})}{\sum_{j=1}^{k}\pi_j N(\boldsymbol{x};\boldsymbol{\mu_{jX}},\delta_{jXX})} \quad (5)$$

3.2 Stomatal conductance models

Both Penman-Monteith and mass transfer equation models require stomatal resistance r_s [m/s] and aerodynamic resistance r_a [m/s]. Because stomatal resistance r_s is much larger than aerodynamic resistance r_a, the aerodynamic resistance was ignored in the calculation without compromising modeling results. Jarvis [56] and the Ball [57] models are the most widely used models for stomatal conductance g_s (the inverse of stomatal resistance). Both models require experimental data to train the coefficients in mathematical functions. Ball model was established based on assimilation rates, relative humidity at the leaf surface, and CO_2 mole fraction while the Jarvis model was established based on environmental conditions such as radiation I, temperature T, vapor pressure deficit (VPD), leaf water potential φ, carbon dioxide concentration C_a. Therefore, the Jarvis model is more suitable for use in this study. Jarvis model (Eq. 6) uses a generalized multiplicative form between stomatal conductance g_s and its mathematical functions with key environmental conditions.

$$g_s = f(I)h(T)i(VPD)j(\varphi)k(C_a) \quad (6)$$

In addition, a GMR model, as described in 3.1.3, was also used to predict the stomatal conductance of indoor plants. The modeling results were illustrated in 3.3.

3.3 Model development and testing results

A Jarvis model was first developed for stomatal conductance using experimental data based on environmental parameters including net radiation (R_n), air temperature (T_a), CO_2 concentration C_a, and vapor pressure deficit (VPD). The R^2 of the Jarvis model (Eq. 7) for stomatal conductance was 0.82 with the coefficient of the variation of the root mean square errors (CV-RMSE) of 36% and the mean bias error (MBE) of 21%. The individual functions (Eqs.8-11) are linear for the environmental parameters except that the function for VPD is logarithmic. The comparison between measured and predicted stomatal conductance from the Jarvis model is shown in Figure 6. It is observed that the deviations between measurement and prediction became large with the increase of stomatal conductance.

$$g_s = f(R_n)h(T_a)i(VPD)k(C_a) \quad (7)$$

$$f(R_n)=0.0045R_n+0.4312 \ (R^2 = 0.77) \quad (8)$$

$$h(T_a)= -0.029T_a + 1.5321 \ (R^2 = 0.02) \quad (9)$$

$$i(VPD)=-0.526 \ LN(VPD)+0.9986 \ (R^2 = 0.009) \quad (10)$$

$$k(C_a) = -0.0007C_a + 1.3303 \ (R^2 = 0.17) \quad (11)$$

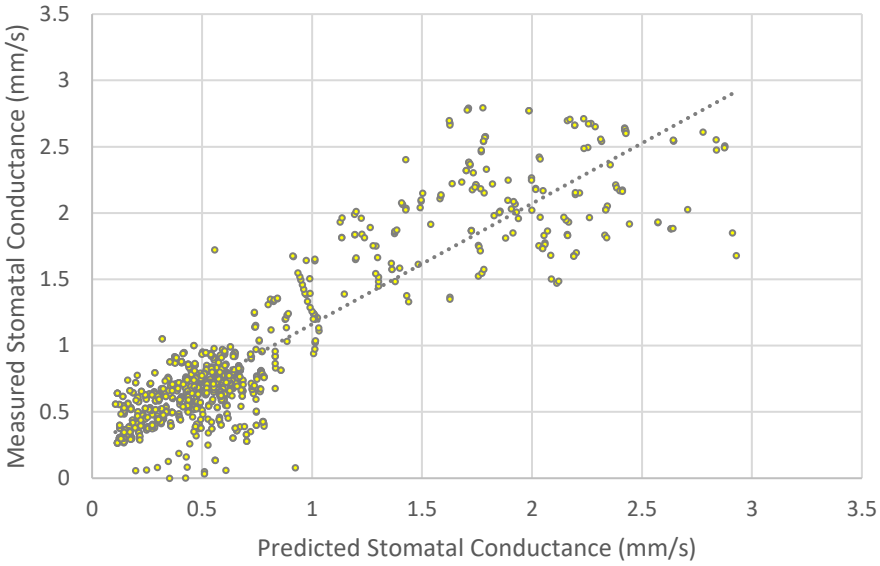

Figure 6. Comparison between predicted and measured stomatal conductance for indoor plants.

Using the Jarvis model for stomatal conductance, Penman-Monteith and mass transfer models were applied for ET prediction. The comparison results are shown in Figure 7 with CV-RMSEs of 42% and 37% and MBEs of 30% and 24% for the Penman-Monteith ET model and mass transfer ET model, respectively. Both models have an R^2 of 0.84. Although the mass transfer ET model has better statistical indices than the Penman-Monteith ET model, CV-RMSE and MBE do not meet the requirements of ASHRAE Guideline 14 [65]. This is mainly due to the less accurate prediction of stomatal conductance from the Jarvis model.

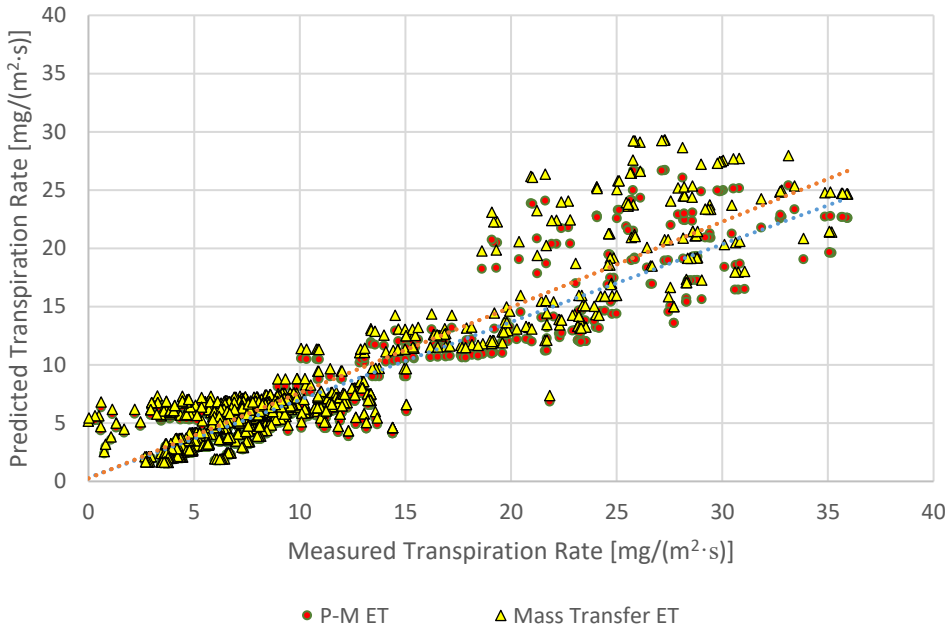

Figure 7. Comparison between measured and predicted transpiration rates with Penman-Monteith and mass transfer ET models

A GMR model was developed to predict stomatal conductance and ET rates based on experimental data. The same set of input parameters as those in the Jarvis model including net radiation (R_n), air temperature (T_a), CO_2 concentration (C_a), and VPD was used for both stomatal conductance and ET prediction. There are 1,113 data points in total, in which 557 data points were used for training and 556 data points were used for testing. The comparison between measured and predicted transpiration rates from a GMR model was shown in Figure 8. CV-RMSEs of 17% and 24% were obtained for ET and stomatal conductance predictions using testing data, respectively. MBEs of -0.7% were obtained for both ET and stomatal conductance predictions. An R^2 of 0.935 was obtained for the testing data. In comparison with the Penman-Monteith and mass transfer ET models, the GMR models have better performance.

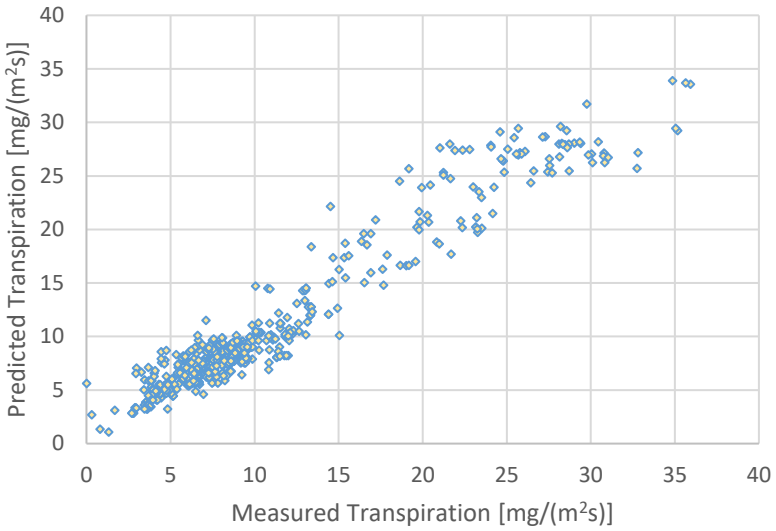

Figure 8. Comparison between measured and predicted transpiration rates from a GMR model.

4. Coupling the indoor living wall model and EnergyPlus model

An indoor living wall model was coupled with the EnergyPlus simulation model through the Python plugin of EnergyPlus. The Python plugin and API features extend the flexibility of using EnergyPlus for hybrid modeling and advanced controls. Customized simulation modules are not necessarily added to EnergyPlus. To expand its functionality, EnergyPlus users can write Python codes to connect with EnergyPlus for co-simulation via Python plugin or API features. In this study, EnergyPlus interacts with the indoor living wall model built upon the GMR model for ET prediction to quantify the effect of the ET process on cooling energy use and the indoor environment.

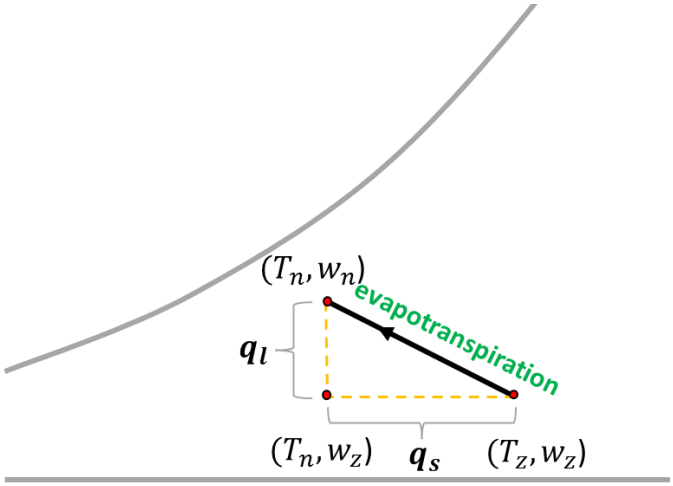

Figure 9. Psychrometric illustration of evapotranspiration (ET) process

As shown in Figure 9, an evapotranspiration (ET) process can be considered as evaporative cooling with nearly constant enthalpy throughout the process. Within each timestep,

the starting moist air condition of a thermal zone (initial zone temperature T_z and initial humidity ratio W_z) will be updated with the addition of moisture from the ET process to a new moist air condition (new zone temperature T_n and new humidity ratio W_n) without the consideration of other internal heat gains as well as energy input from HVAC systems. The ET process from indoor living walls can be interpreted as add-on sensible (q_l) and latent loads (q_s) influencing the indoor heat balance of EnergyPlus.

The algorithm for modeling indoor living walls was illustrated using a flow chart (Figure 10). Four key parameters including net radiation, air temperature, CO_2 concentration, and VPD were first processed as input parameters of the ET model. The illuminance level was treated as plant net radiation and was calculated as the illuminance level of a specified distance from windows at 1.0 m height above the floor. Indoor CO_2 concentration was assumed as a constant at 400 ppm. This is a reasonable assumption for most spaces with adequate ventilation. In addition, ET rates were relatively stable when CO_2 concentration ranges between 400 ppm and 500 ppm based on measurements. The thermal zone air temperature was retrieved from the end of the previous timestep. VPD was calculated based on air temperature and relative humidity retrieved from the end of the previous timestep. The predicted ET rate based on the GMR model was used to update the humidity ratio of each timestep (Eq. 12).

$$W_n = W_z + \frac{ET \times LA \times t}{\rho \times V \times 10^6} \qquad (12)$$

Where ET [mg/(m^{2}s)] is the evapotranspiration rate per unit area, LA [m^2] represents the total leaf area of indoor living walls, ρ [kg/m^3] is the dry air density, and V [m^3] is thermal zone volume, W_z [kg H_2O/kg dry air] is the zone air humidity ratio at the end of the previous timestep, and W_n [kg H_2O/kg dry air] is the updated zone air humidity ratio after the ET process.

Then the updated humidity ratio W_n [kg H_2O/kg dry air] is compared to the humidity ratio W_s of the saturated condition. If W_n is greater than W_s, the moist air is in a saturated condition, and the updated zone air temperature T_n is equal to the zone wet-bulb temperature. Otherwise, the zone air temperature T_n can be calculated based on W_n and zone air enthalpy h_z [kJ/kg dry air]. The assumption is that zone air enthalpy before and after the ET process stays nearly constant as an evaporative cooling process. We then calculate equivalent sensible and latent loads due to ET influencing the thermal zone heat balance of EnergyPlus based on Fig. 9.

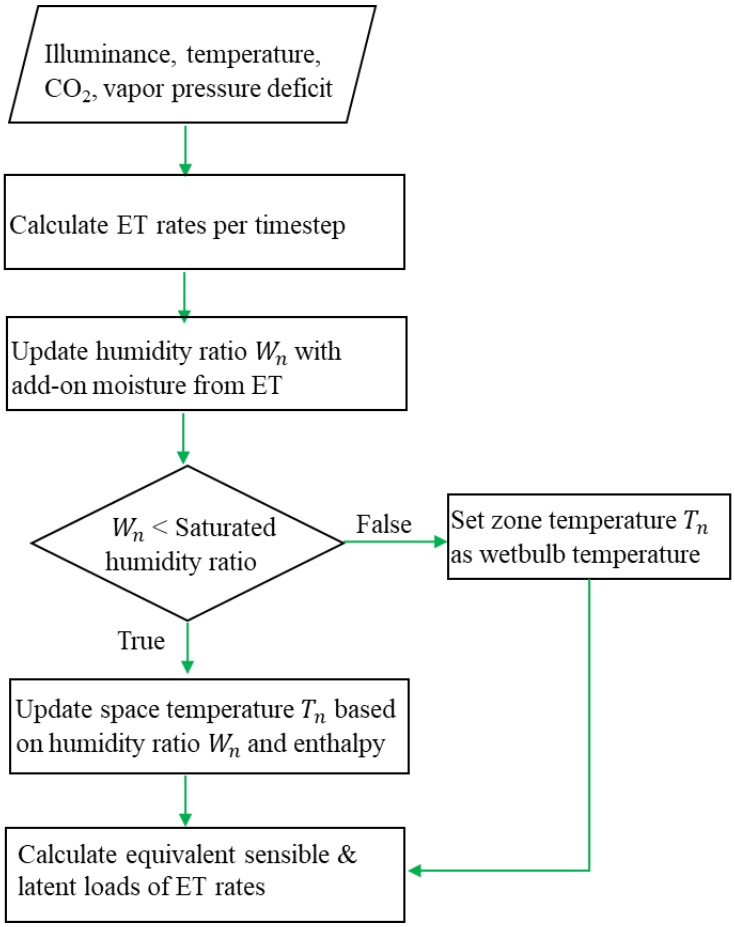

Figure 10. A flowchart of the indoor living wall model

The approach using Python plugin enables ET modeling with complex machine learning methods. However, the effects of indoor living walls on zone heat balance were not fully addressed. The proposed modeling approach only simulated the ET effect from indoor living walls on thermal zone energy balance. In addition to the influence of the ET process, convection and radiation effects between plant surface and zone air should also be considered as part of the effects from living walls. A new module on indoor living wall systems in energy simulation software such as EnergyPlus would still be necessary for comprehensively considering the effects of indoor living walls on building energy use and space temperature convergence between the indoor living wall model and heat balance. Due to the nature of external coupling, the integrated program took much longer to run in comparison with running EnergyPlus alone.

5. EnergyPlus model and parametric runs

The DOE medium-sized office building reference model was modified and used in this study to evaluate indoor living walls' impacts on cooling energy use. The building reference model was developed in compliance with ASHRAE 90.1-2007 [53]. The medium-sized office building has five thermal zones per story and three stories in total. The thermal zone layout of

each floor is shown in Figure 11. The window to wall ratio (WWR) for each orientation is 0.33. The building was served by three multi-zone variable air volume (VAV) systems (one system for each floor) with direct expansion (DX) coils for cooling and gas burners for heating. Each VAV terminal unit has an electric reheating coil. A constant of 30% was set for the minimum airflow fraction of VAV terminal units in the original model. The cooling setpoint was 24ºC during occupied hours and 26.7ºC during unoccupied hours. The heating setpoint was 21ºC during occupied hours and 15.6ºC during unoccupied hours.

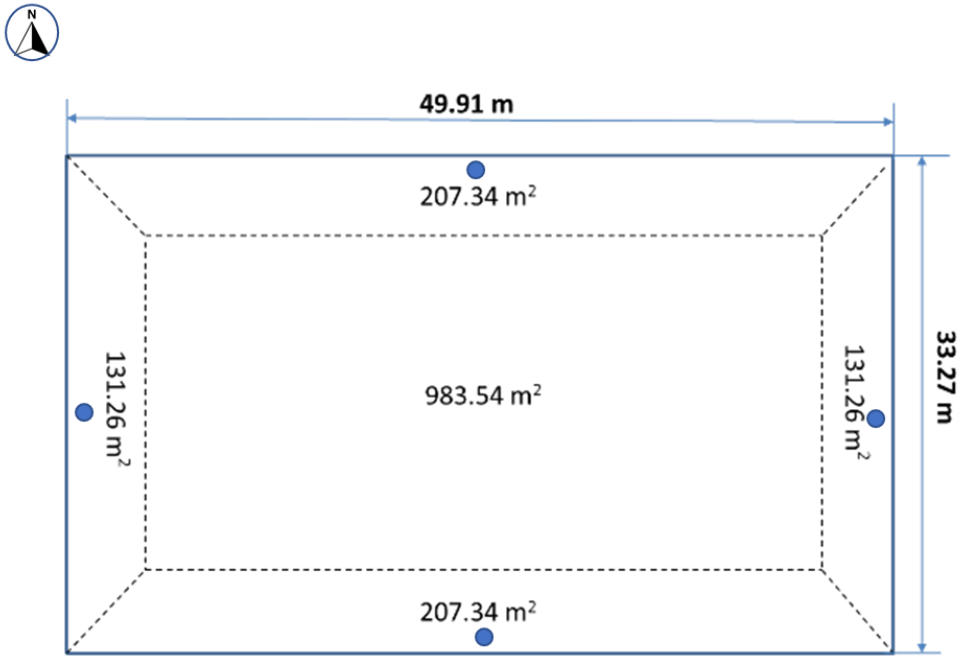

Figure 11. Thermal zone layout and daylighting reference points for the medium-sized office building prototype in EnergyPlus

To meet the objective of this study for evaluating indoor living walls' impacts on cooling energy use in commercial buildings, the DOE medium-sized office building reference model was modified as follows. First, use a constant cooling setpoint of 24ºC throughout the day. Second, set the minimum airflow fraction of VAV terminal units as autosize in EnergyPlus to meet ventilation requirements from ASHRAE Standard 62.1[66]. Third, add daylighting reference points (Figure 11) for capturing the illuminance level of a specified distance from the exterior window at 1.0 m height from the floor for each perimeter zone.

A parametric study on the leaf area to floor area ratios (LFAR), orientations, distances from windows, and climates was conducted to evaluate the influence of each factor on indoor living walls' performance. LFAR is defined as the ratio between the total leaf area of indoor living walls to the floor area of a thermal zone. Indoor living walls were placed in each perimeter zone for four different orientations (N, S, W, E) of the middle floor and at different distances including 0.5 m, 1.0 m, 1.5 m, 2.0 m, 2.5 m, 3.0 m, 3.5 m, 4.0 m and 4.5 m from windows. Nine leaf-to-floor-area ratios including 0.1, 0.3, 0.5, 0.8,1.0,1.5, 2.0, 2.5, 3.0 were simulated and tested in this study. In addition, parametric simulations for three ASHRAE Climate Zones: 1A (very hot and humid), 2B (hot and dry), and 3B (warm and dry) were run for summer design days

using the integrated EnergyPlus and indoor living wall model simulation. The representative cities are Miami, FL, Phoenix, AZ, and Los Angeles, CA for 1A, 2B, and 3B, respectively. Summer design days are 7/21 for Miami and Phoenix and 8/21 for Los Angeles. In total, 243 models with indoor living walls and 24 models with both indoor living walls and humidity control were simulated using EnergyPlus. In each model, the effects of indoor living walls were evaluated for the four perimeter zones simultaneously. A separate Python code was developed to automatically update the EnergyPlus models and associated python codes for EnergyPlus plugin.

6. Results

Simulation results are presented and analyzed for the medium-sized office building with indoor living walls for two control options: temperature control only, and temperature and humidity control.

6.1 Simulation result analysis for indoor living walls with temperature control only

Living walls' effects on cooling energy use in the medium-sized office building were evaluated from the influential factors: climates, orientations, distances from windows, and LFARs. Percentage of cooling rate reduction for perimeter zones, indoor environmental conditions including zone air temperature and relative humidity, and ET rates were analyzed for different scenarios.

6.1.1 Climates

The scenarios with living walls placed 1.0 m from the window of the south perimeter zone and LFAR=0.8 were used to illustrate the cooling effects in different climates. Cooling energy uses were reduced by 3.4% (4.3 kWh), 3.6% (5.1 kWh), and 7.6% (9.1 kWh, for Miami (MI), Phoenix (PH), and Los Angeles (LA), respectively on the design day. For unit area (m^2) of indoor living walls, cooling energy savings were equivalent to 0.026 kWh/m^2 of living wall/zone, 0.031 kWh/m^2 of living wall/zone, and 0.055 kWh/m^2 of living wall/zone for MI, PH, and LA, respectively. Figure 12 compares the cooling rates between baseline without indoor living walls and the living wall scenarios with LFAR=0.8 in the south perimeter zone. As shown in Figure 12, cooling reductions mainly occurred in the morning between 8:00 am -10:00 am and late afternoon 2:00 pm – 4:00 pm. As shown in Figure 13, ET rates were mostly influenced by net radiation (illuminance level at reference point). The illuminance level in EnergyPlus for each reference point was measured in lux, which is converted to photosynthetically active radiation (PAR) in W/m^2 (1 W/m^2=126 lux). Because the illuminance level in LA is the highest among the three climates on design days, cooling reduction in LA is the highest among the three cities. Figure 14 shows that zone air temperatures stayed at a constant of 24 ºC as required by the cooling setpoint and zone relative humidity was in a reasonable range with living wall scenarios for all three climates.

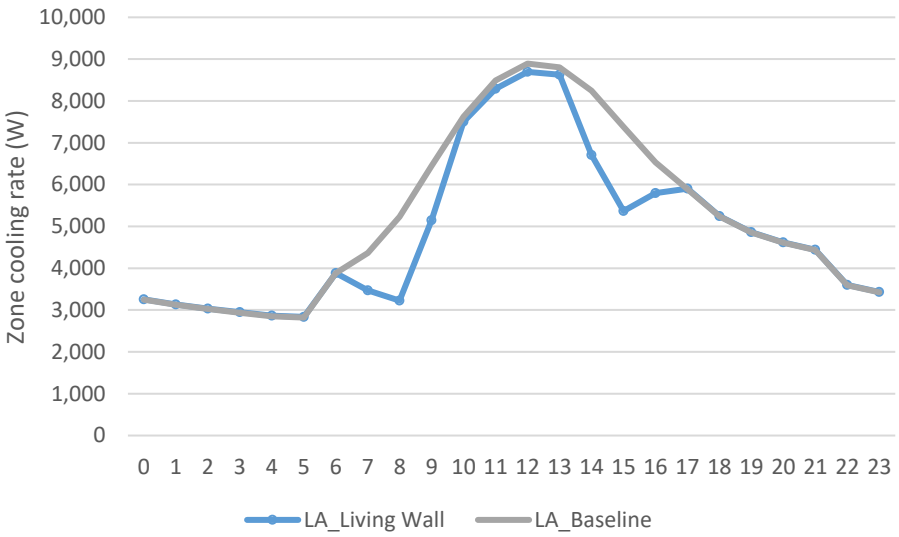

Figure 12. Comparison of hourly-averaged cooling rates between baseline and living wall scenario with LFAR=0.8 and 1.0 from the window of the south perimeter zone in LA

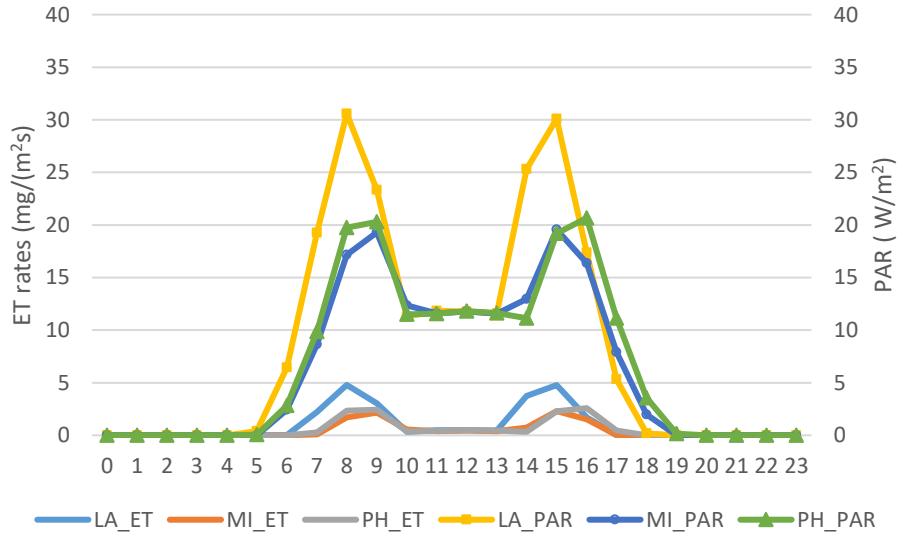

Figure 13. Hourly-averaged ET rates and photosynthetically active radiation (PAR) at 1.0 m from the window of the south perimeter zone

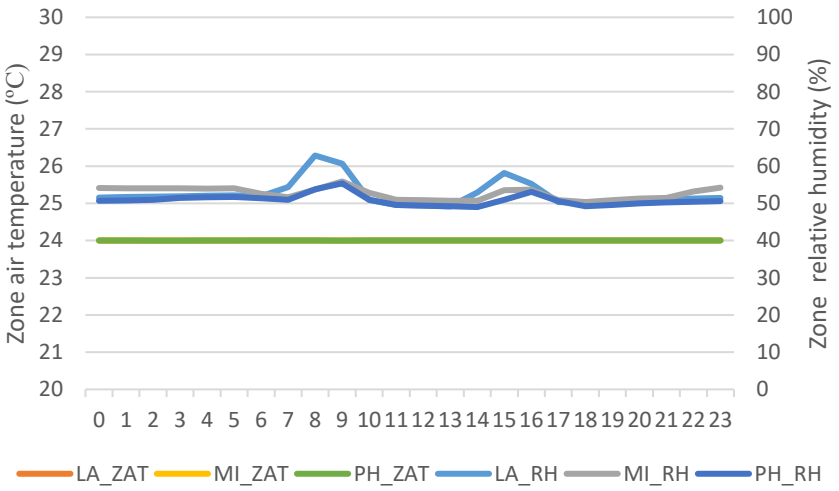

Figure 14. Hourly-averaged zone air temperature and relative humidity for living wall scenario with LFAR=0.8 and 1.0 m from the window of the south perimeter zone (note: ZAT—zone air temperature, RH—relative humidity).

6.1.2 Orientations

Reduced percentage of cooling rates were compared for the four perimeter zones with different orientations (north, south, west, and east). Figure 15 showed the cooling rate reductions for different oriented perimeter zones with LFAR=1.0 at 0.5 m from windows. In all three climates, cooling rates were reduced by 22.7%-25.4% (23.5 kWh – 26.3 kWh) and by 19.1%-22.2% (20.3 kWh – 22.1 kWh) for the west and east perimeter zones, respectively; cooling rate reductions were relatively small ranging from 3.4% to 6.9% (3.6 kWh – 9.4 kWh) for the north perimeter zones. The percentage of cooling rate reduction ranges from 3.4% to 27.4% (4.5 kWh – 34.5 kWh) with a large difference for south perimeter zones mainly due to different illuminance levels which affect ET rates.

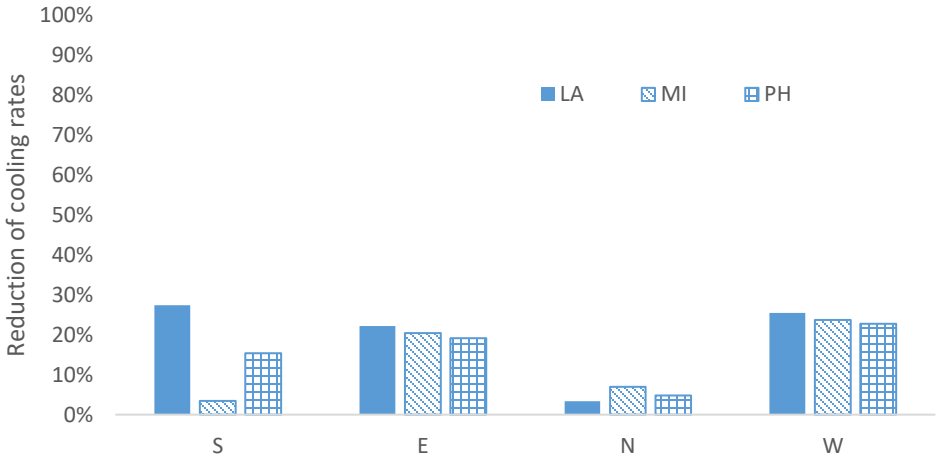

Figure 15. Cooling rate reductions for different oriented perimeter zones with LFAR=1.0 at 0.5 m from windows.

Hourly-averaged space air temperature and relative humidity of perimeter zones were illustrated in Figure 16 for living wall scenarios with LFAR=1.0 and 0.5 m from the window in PH. Space air temperature stayed at a constant 24ºC for most of the time except early morning in the east perimeter zone and afternoon in the west perimeter zone. This is because the cooling effects from the ET process for the two perimeter zones are sufficient to cool off the space during those periods with required mechanical ventilation as shown in Figure 17 for the west perimeter zone between 2:00 pm and 3:00 pm was due to space ventilation requirement. It is also noted that space relative humidity was significantly increased in the early morning of the east perimeter zone and late afternoon of the west perimeter zone and throughout the day for the south perimeter zone in PH due to the ET process.

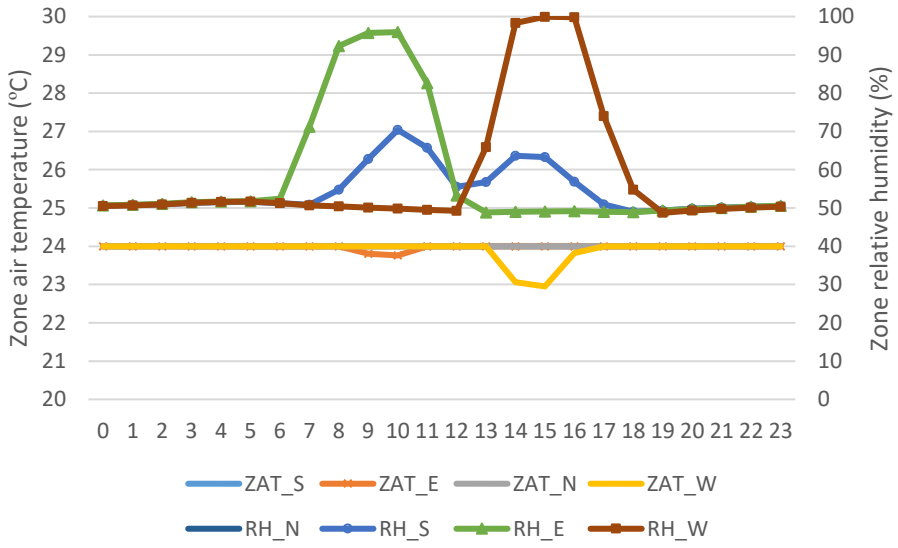

Figure 16. Hourly-averaged zone air temperature and relative humidity for living wall scenario with LFAR=1.0 and 0.5 m from the window in PH (note: ZAT—zone air temperature, RH—relative humidity, _S—south perimeter zone, _E—east perimeter zone, _N—north perimeter zone, _W—west perimeter zone).

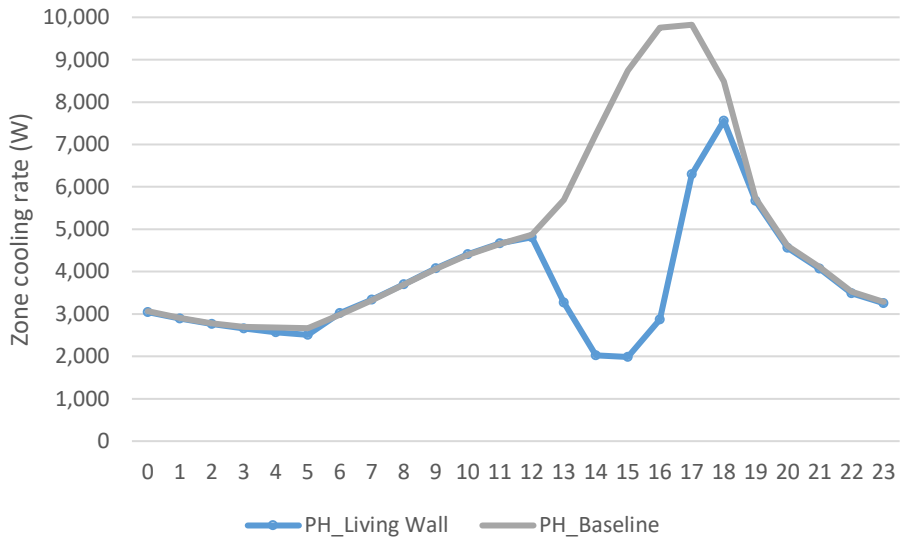

Figure 17. Comparison of cooling rates between baseline and living wall scenario with LFAR=1.0 and 0.5 m from the window of west perimeter zone in PH

6.1.3 Distance from windows

The distance of living walls from windows in perimeter zones plays an important role. Generally speaking, when living walls were placed close to exterior windows, the living walls receive high radiation; when living walls were placed further away from windows, the living walls receive relatively low radiation. However, due to the fact that daylight was reflected from space surfaces, the illuminance levels may not always reduce with the increased distance from the window. Figure 18 illustrated the variation of cooling rate reduction with the change of the living walls' distances from windows when LFAR=1.0 for the south perimeter zone. When living walls were placed close to exterior windows, the cooling rate reduction can be substantially high (27.4% for LA and 15.3% for PH). Per unit area of indoor living walls, the cooling energy savings were 0.17 kWh/m^2 of living wall /zone for LA, and 0.11 kWh/m^2 of living wall/zone for PH on the design day. When living walls were placed close to the interior walls, the cooling rate reduction was only 1.2%-1.5%. When living walls were placed within 2.5 m from exterior windows, the average cooling rate reductions for the south perimeter zone were 4.5% (5.9 kWh) for MI,6.5% (9.4 kWh) for PH, and 10.1% (12.7 kWh) for LA.

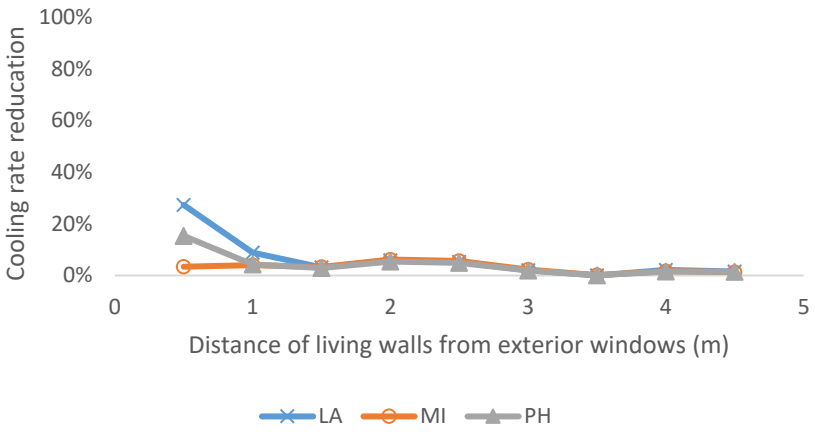

Figure 18. Cooling rate reductions with the change of living walls' distances from windows for scenarios with LFAR=1.0 for the south perimeter zone.

6.1.4 Leaf to floor area ratio (LFAR)

LFARs ranging from 0.1 to 3.0 were evaluated for the cooling effects of living walls. Figure 19 showed the variation of cooling rate reductions with the change of LFAR for living walls placed 0.5 m from windows in LA. With the increase of leaf area ratio, cooling rate reduction for perimeter zones has been increased. It can be seen that up to 41.2% (51.9 kWh) of the cooling rate can be reduced for the south perimeter zone in LA when living walls were placed close to the window with a leaf area ratio of 3.0. The maximum cooling rate reduction was 36.4% (33.7 kWh) and 35.1% (32.1 kWh) for the west and east perimeter zones, respectively.

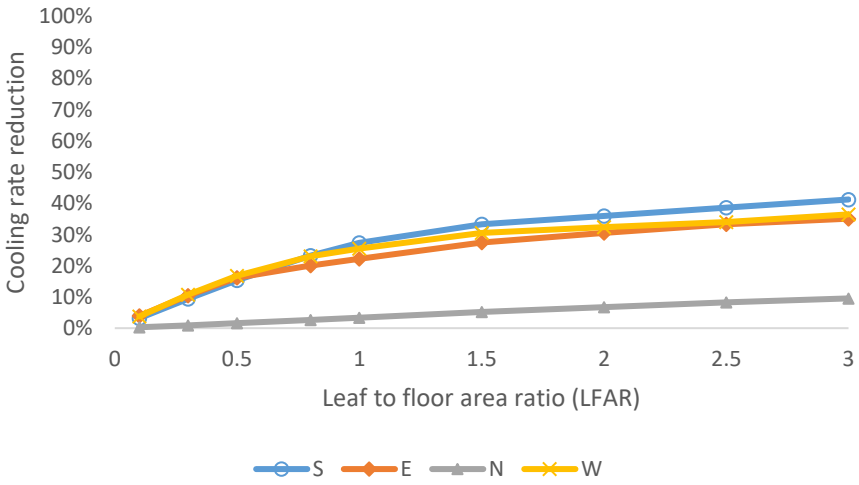

Figure 19. Cooling rate reductions with the change of LFARs for living walls placed 0.5 m from windows in LA. (note: S—south perimeter zone, E—east perimeter zone, N—north perimeter zone, W—west perimeter zone).

However, with the increase of LFARs, periods when space relative humidity exceeds 85% were also increased as shown in Table 1. For example, 7.7% of the design day exceeding 85% relative humidity represented about 1.8 hours of the design day. If 34.9% of the time exceeds 85% relative humidity (8.4 hours), the exceeding period would be too high. A designer should select a suitable LFAR or have both temperature and humidity control for spaces to avoid high space relative humidity over a long period. By adding humidity control with dehumidification at system or zone levels, the cooling rate reduction would be compromised and optimization could be performed to identify the best design solution for a specific building design. Natural ventilation or mixed-mode ventilation could be an interesting accompanying strategy with indoor living walls to reduce issues with high relative humidity and achieve further energy savings.

Table 1. Percentage of time when space relative humidity was higher than 85% when indoor living walls were placed 0.5 m from windows on the design day in LA.

LFAR / Orientation	**0.1**	**0.3**	**0.5**	**0.8**	**1**	**1.5**	**2**	**2.5**	**3**
S	0.0%	0.0%	0.0%	0.6%	7.7%	29.0%	32.4%	34.0%	34.9%
E	0.0%	0.0%	7.5%	13.4%	15.1%	18.6%	19.7%	19.3%	17.3%
N	0.0%	0.0%	0.0%	0.0%	0.0%	0.0%	0.0%	0.0%	0.0%
W	0.0%	0.0%	8.0%	12.6%	14.1%	18.1%	19.0%	19.2%	19.7%

6.2 Simulation result analysis for indoor living walls with both temperature and humidity control

To properly control indoor space humidity levels, a humidistat of 80% relative humidity as the upper limit was added to each perimeter zone of the middle floor in the EnergyPlus model. In addition, a DX dehumidifier with a rated water removal of 300 L/day and a rated energy factor of 3.412 L/kWh was added to the EnergyPlus models for each perimeter zone to remove extra moisture from living wall for thermal comfort. 24 parametric runs were conducted for the three climates with eight LFARs (0.3, 0.5, 0.8, 1, 1.5, 2, 2.5, 3) when living walls were placed 0.5 m from the exterior windows.

6.2.1 Performance comparison with and without dehumidification device

The scenario—LFAR=1.0 with indoor living walls placed 0.5 m from the windows in LA—was used as an example to illustrate the performance with and without dehumidification devices. The performance parameters for comparison include DX cooling coil electricity rates, ET rates, and relative humidity.

With the addition of DX dehumidification devices, periods of high relative humidity for perimeter zones were reduced. Figures 20 (a)-(c) showed the hourly-averaged space relative humidity for the south, east, and west perimeter zones with LFAR=1.0. The percentage of time exceeding 85% relative humidity was reduced from 7.7% to 0.6% for the south perimeter zone, from 15.1% to 2.8% for the east perimeter zone, and from 14.1% to 4.8% for the west perimeter zone.

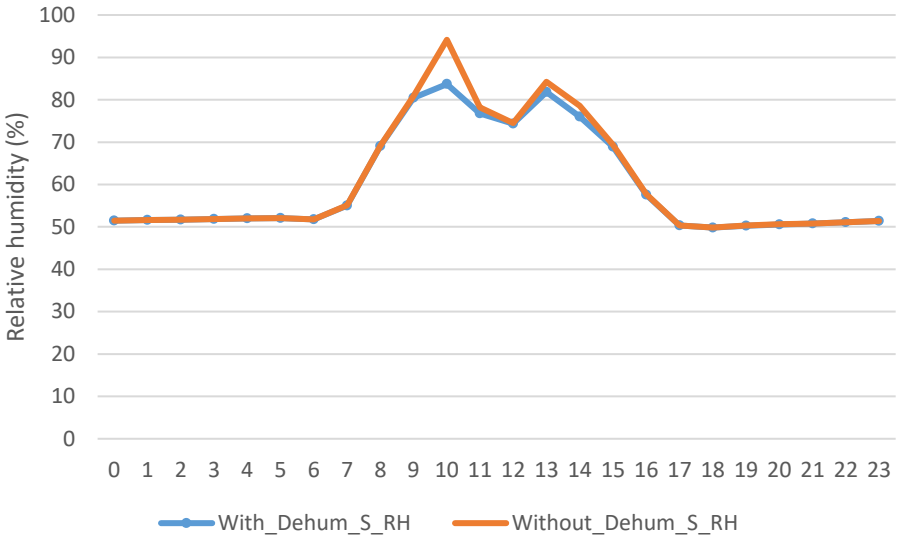
Relative humidity (%)
100
90
80
70
60
50
40
30
20
10
0
0 1 2 3 4 5 6 7 8 9 10 11 12 13 14 15 16 17 18 19 20 21 22 23
With_Dehum_S_RH
Without_Dehum_S_RH

(a)

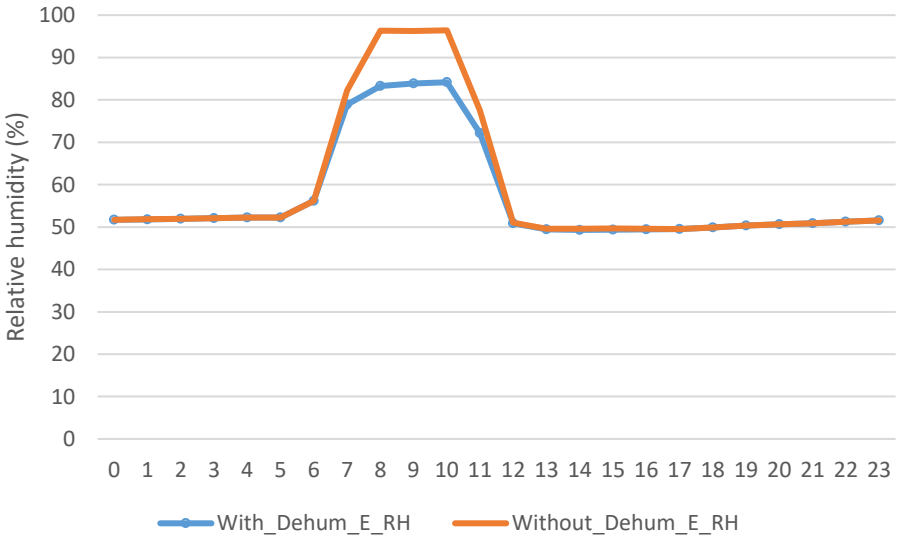
Relative humidity (%)
100
90
80
70
60
50
40
30
20
10
0
0 1 2 3 4 5 6 7 8 9 10 11 12 13 14 15 16 17 18 19 20 21 22 23
With_Dehum_E_RH
Without_Dehum_E_RH

(b)

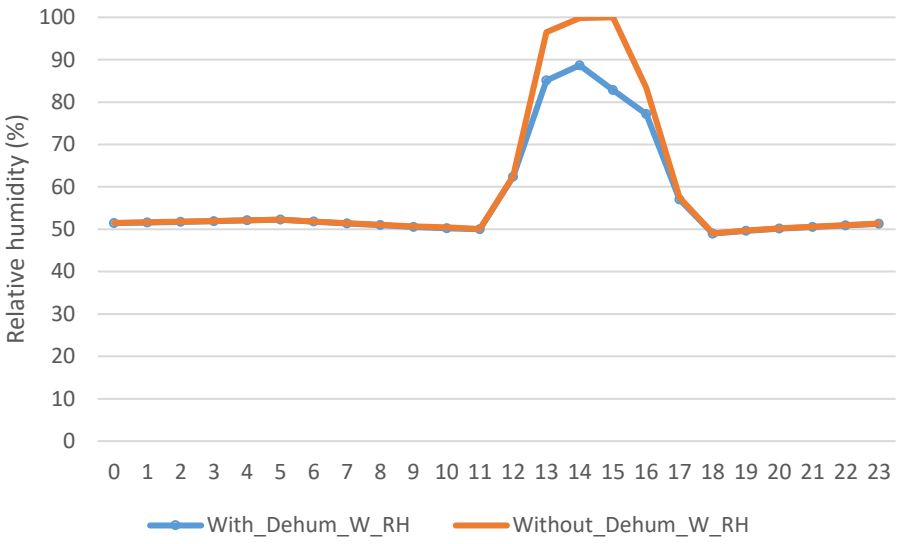

(c)

Figure 20. Hourly-averaged space relative humidity: a. south perimeter zone, b. east perimeter zone, c. west perimeter zone for LFAR=1.0 with indoor living walls placed 0.5 m from the windows in LA (note: RH—relative humidity, _S—south perimeter zone, _E—east perimeter zone, _W—west perimeter zone).

Hourly-averaged ET rates for the south perimeter zone, east perimeter zone, and west perimeter zone were shown in Figures 21 (a)-(c). There were negligible increases in ET rates for south and east perimeter zones while ET rates were increased by 13% for west perimeter zones with the addition of DX dehumidification. The controlled relative humidity resulted in the VPD increase, and therefore the increase in ET rates.

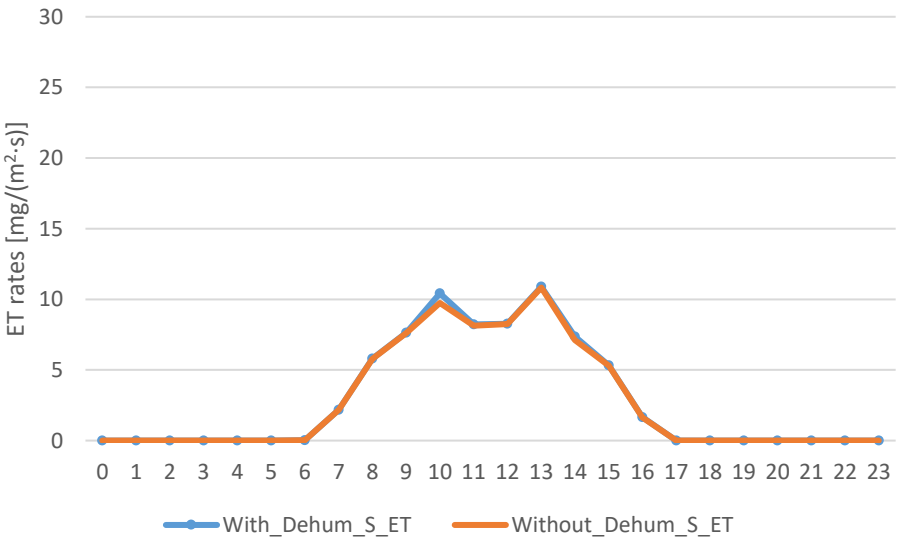

(a)

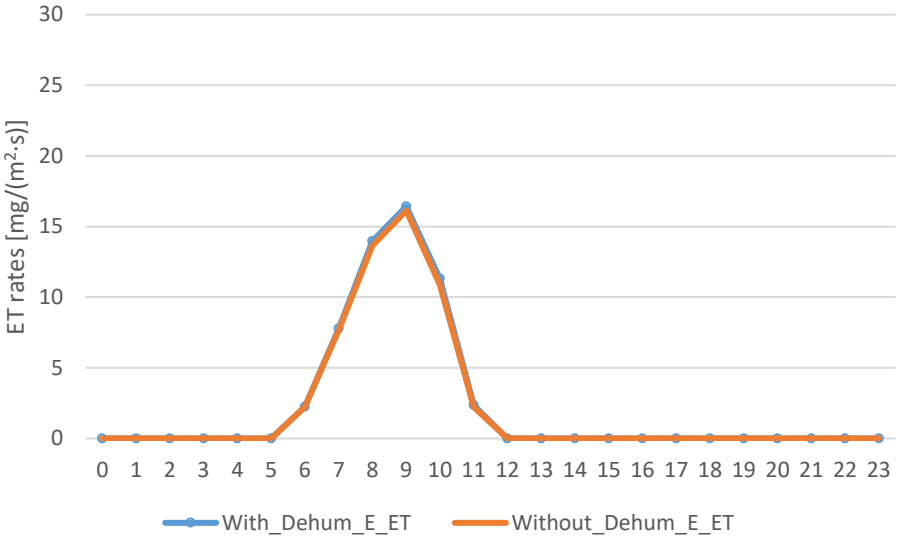

(b)

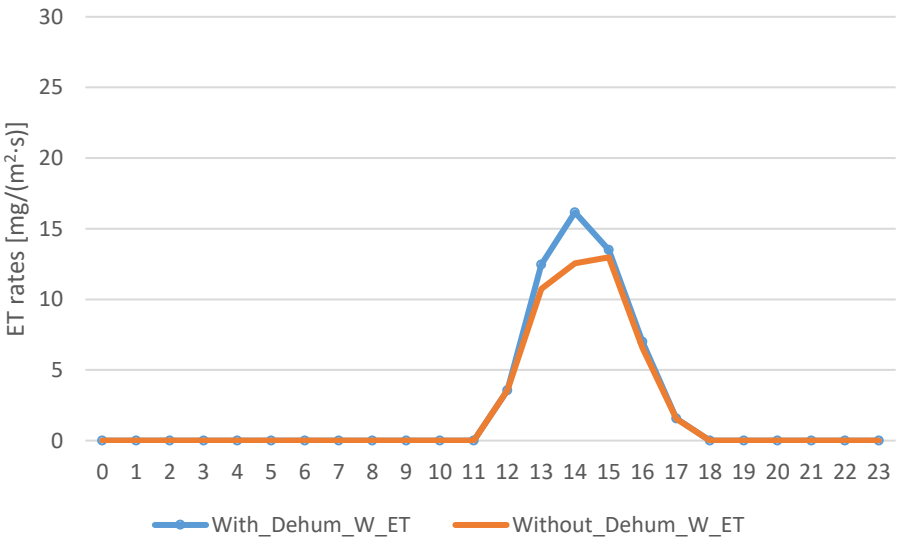

(c)

Figure 21. Hourly-averaged ET rates: a. south perimeter zone, b. east perimeter zone, c. west perimeter zone for LFAR=1.0 with indoor living walls placed 0.5 m from the windows in LA (note: _S—south perimeter zone, _E—east perimeter zone, _W—west perimeter zone).

The five thermal zones (four perimeter zones and one core zone) on the middle floor were served by a VAV system with a DX cooling coil for cooling. Figure 22 showed the DX cooling coil electricity rates for the VAV system in three scenarios: baseline (no living walls and no DX dehumidification), the scenario with living walls and DX dehumidification, and the scenario with living walls only. With the indoor living walls (LFAR=1.0) placed in each

perimeter zones, the electricity use savings from the DX cooling coil were 9.2% (38.0 kWh) for the scenario with living walls only and 6.7% (27.9 kWh) for the scenario with living walls and DX dehumidification on the design day. In comparison with the scenario with living walls only, there were increases in DX coil electricity use (10.1 kWh) for the scenario with living walls and DX dehumidification. The increases in DX coil electricity use were due to the add-on sensible reheat generated by the DX dehumidification process.

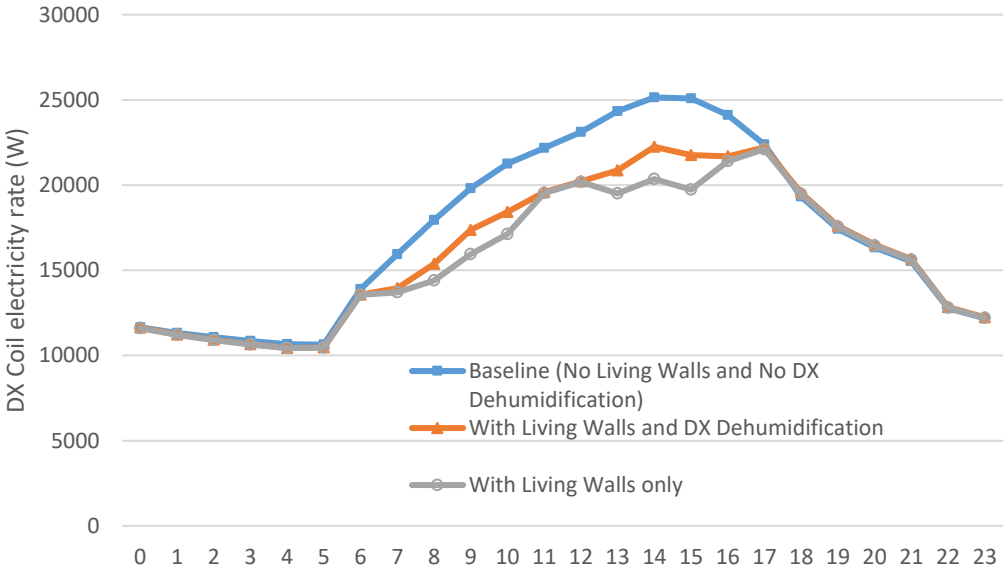

Figure 22. Hourly-averaged DX cooling coil electricity rates for thermal zones on the middle floor of the prototype building for LFAR=1.0 with indoor living walls placed 0.5 m from the windows in LA.

6.2.2 Cooling electricity savings

In addition to the analysis of direct system cooling rate reduction as discussed in section 6, the impacts of indoor living walls on cooling electricity use on the design day were evaluated for different scenarios.

Cooling electricity savings from the benefits of living walls were compared for scenarios with different LFARs in LA on the design day. Total electricity use for the middle floor includes the fan, DX cooling, and DX dehumidifiers. In this study, the cooling electricity savings for each perimeter zone were obtained based on the steps as follows. First, the cooling electricity use of the middle floor system was allocated for each thermal zones as zone-level cooling electricity use based on the proportion of cooling loads among the five thermal zones including the core zone and the four perimeter zones for both baseline models and models with living walls and DX dehumidification. Second, the absolute electricity savings were calculated as the difference of cooling electricity use of the perimeter zone between baseline and the scenario with living walls subtracted by the extra electricity use of the DX dehumidifier for each perimeter zone. Third, the percentage savings of cooling electricity use for each perimeter zone were calculated as the absolute electricity savings divided by the electricity use of each perimeter zone in the baseline.

Table 2. Percentage of savings in cooling electricity use when indoor living walls were placed 0.5 m from windows on the design day in LA.

LFAR / Orientation	**0.3**	**0.5**	**0.8**	**1**	**1.5**	**2**	**2.5**	**3**
S	9.0%	14.4%	21.0%	24.3%	25.1%	23.1%	19.1%	14.3%
E	10.0%	14.4%	12.6%	10.5%	3.4%	2.6%	5.4%	5.8%
N	0.4%	0.4%	-0.2%	-0.5%	-2.3%	-1.6%	-0.6%	0.4%
W	10.3%	14.5%	14.3%	13.2%	5.5%	2.0%	0.5%	-0.1%

With the increase of living wall areas, although the cooling rates were continuously reduced (Figure 19), the periods of high relative humidity were also increased (Table 1). Therefore. DX dehumidification devices were added to the perimeter zones to control space relative humidity. Table 2 showed the percentage of savings in cooling electricity use for each perimeter zone for the living wall scenarios with different LFARs. With the consideration of extra electricity use from DX dehumidification devices, the maximum cooling electricity savings in LA are 25.1% (16.2 kWh, 0.052 kWh/m^2 of living wall/zone) when LFAR=1.5 for the south perimeter zone, 14.4% (6.8 kWh, 0.103 kWh/m^2 of living wall/zone) when LFAR=0.5 for the east perimeter zone, 0.3% (0.2 kWh, 0.004 kWh/m^2 of living wall/zone) when LFAR=0.3 for the north perimeter zone, and 14.5% (6.8 kWh, 0.104 kWh/m^2 of living wall/zone) when LFAR=0.5 for west perimeter zone on the design day.

Table 3. Percentage of time when space relative humidity was higher than 85% when indoor living walls were placed 0.5 m from windows on the design day in LA.

LFAR / Orientation	**0.3**	**0.5**	**0.8**	**1**	**1.5**	**2**	**2.5**	**3**
S	0.0%	0.0%	0.0%	0.2%	3.5%	8.2%	11.5%	14.6%
E	0.0%	0.0%	0.9%	3.0%	3.3%	7.8%	10.3%	10.4%
N	0.0%	0.0%	0.0%	0.0%	0.0%	0.0%	0.0%	0.0%
W	0.0%	0.0%	2.4%	3.3%	2.6%	10.5%	14.0%	14.2%

Table 3 showed the percentage of time when space relative humidity exceeds 85%. In comparison with Table 1, the periods with high relative humidity were substantially reduced. However, there were still periods when relative humidity exceeds 85% due to the excess amount of moisture added to the space from living walls. If we consider both cooling electricity savings and periods with high relative humidity, we would recommend LFAR=1 with 24.3% of cooling electricity savings (15.6 kWh, 0.075 kWh/m^2 of living wall/zone) for the south perimeter zone instead of LFAR=1.5 based on the design day simulation.

7. Conclusion

Indoor living walls become increasingly used in building designs and remodeling from aesthetic and well-being perspectives. Currently, indoor greenery systems and building systems

are disconnected in their design stages. The cooling effects of indoor living walls have not been considered or quantified. This study represents the first in developing a modeling method for quantifying the impacts of indoor greenery systems on building cooling energy consumption.

A GMR ET model was developed based on measurement data from the portable photosynthesis system LI-6400XT. An indoor living wall model quantifying sensible and latent loads from the ET process was developed in python. Real-time data exchange between the indoor living wall model and an EnergyPlus model for every timestep was achieved through one of the advanced features Python plugin of EnergyPlus. The proposed modeling approach only simulated the ET effect from indoor living walls on thermal zone energy balance. Considering the effects of convection and radiation between plant surface and zone air could further improve the accuracy of evaluating indoor living walls' cooling effects.

To obtain noticeable cooling effects, indoor living walls should be placed close to the exterior window of perimeter zones. When LFAR is 1.0 with living walls placed 0.5 m from the exterior window, the cooling rate reduction was 27.4% (34.5 kWh, 0.166 kWh /m^2 of living wall/zone) for the south perimeter zone, 25.5% (23.5 kWh, 0.179 kWh /m^2 of living wall/zone) for the west perimeter zone, and 22.2% (20.3 kWh, 0.155 kWh /m^2 of living wall/zone) for the east perimeter zone in LA on the design day. When LFAR was increased to 3.0, up to 41.2%, 36.4%, and 35.1% of the cooling rate can be reduced for the south, west, and east perimeter zones in LA, respectively. However, extended hours of high space humidity with high LFAR compromise thermal comfort, and dehumidification requirements reduce cooling energy savings.

DX dehumidification devices were added to the models with living walls to control the humidity of perimeter zones. The cooling rate reduction from indoor living walls would be compromised. Savings of cooling electricity use from indoor living walls with the consideration of energy penalty from DX dehumidification were further predicted from EnergyPlus simulations on the cooling design day. For different orientations, the design leaf area ratios should be different. The recommended LFARs are 1.0 for the south perimeter zone with 24.3% cooling electricity use reduction (15.6 kWh, 0.075 kWh/m^2 of living wall/zone), 0.5 for the east perimeter zone with 14.4 % cooling electricity use reduction (6.8 kWh, 0.103 kWh/m^2 of living wall/zone), 0.3 for the north perimeter zone with 0.3% cooling electricity use reduction (0.2 kWh, 0.004 kWh/m^2 of living wall/zone), and 0.5 for the west perimeter zone with 14.5% cooling electricity use reduction (6.8 kWh, 0.104 kWh/m^2 of living wall/zone) in LA.

In this study, only the plant type *Epipremnum aureum* was measured for ET performance. Other types of plants should also be measured to create a database of different plants for a generalized ET model. EnergyPlus daylighting reference points were used to determine the radiation incident on the leaves. Although the radiation varied each time step based on solar radiation, solar angles, and cloud conditions, it was assumed to be the same for all leaves of the indoor living wall system. A further experimental study should be carried out to develop a method for quantifying radiation on shaded leaves and the effect of different incident angles. In addition, the cooling effects of indoor living walls were evaluated for three climates based on a summer design day. In future studies, annual energy simulations will be conducted to comprehensively consider the effects of indoor living walls at different seasons across different

climates. The opportunity of combining mixed-mode ventilation with indoor living walls to reduce issues of high relative humidity and achieve better energy efficiency should also be explored.

Acknowledgment

This study is supported by the National Science Foundation Environmental Sustainability program under Grant No. CBET 1944823. Any opinions, findings, conclusions, or recommendations expressed in this material are those of the authors and do not necessarily reflect the views of the National Science Foundation.

References

1. IPCC, *Climate Change 2014: Synthesis Report. Contribution of Working Groups I, II and III to the Fifth Assessment Report of the Intergovernmental Panel on Climate Change [Core Writing Team, R.K. Pachauri and L.A. Meyer (eds.)]*, 2014.
2. IPCC, *Global Warming of 1.5 ºC: Special Report*, 2018.
3. Wong, N.H., et al., *Thermal evaluation of vertical greenery systems for building walls.* Building and Environment, 2010. **45**(3): p. 663-672.
4. Shafiee, E., et al., *Assessment of the effect of living wall systems on the improvement of the urban heat island phenomenon.* Building and Environment, 2020. **181**: p. 106923.
5. Santamouris, M., *Recent progress on urban overheating and heat island research. Integrated assessment of the energy, environmental, vulnerability and health impact. Synergies with the global climate change.* Energy and Buildings, 2020. **207**: p. 109482.
6. Perini, K., et al., *Vertical greening systems and the effect on air flow and temperature on the building envelope.* Building and Environment, 2011. **46**(11): p. 2287-2294.
7. Susorova, I., et al., *A model of vegetated exterior facades for evaluation of wall thermal performance.* Building and Environment, 2013. **67**: p. 1-13.
8. Ottelé, M., H.D. van Bohemen, and A.L.A. Fraaij, *Quantifying the deposition of particulate matter on climber vegetation on living walls.* Ecological Engineering, 2010. **36**(2): p. 154-162.
9. Weyens, N., et al., *The Role of Plant–Microbe Interactions and Their Exploitation for Phytoremediation of Air Pollutants.* International Journal of Molecular Sciences, 2015. **16**(10).
10. Abtew, W. and A. Melesse, *Evaporation and Evapotranspiration: Measurements and Estimations*2013: Springer.
11. EPA. *Indoor Air Quality: What are the trends in indoor air quality and their effects on human health?* . Available from: https://www.epa.gov/report-environment/indoor-air-quality.
12. Fernandez-Canero, R., L. Perez Urrestarazu, and A. Franco Salas, *Assessment of the Cooling Potential of an Indoor Living Wall using Different Substrates in a Warm Climate.* Indoor and Built Environment, 2011. **21**: p. 642-650.
13. Pérez-Urrestarazu, L., et al., *Influence of an active living wall on indoor temperature and humidity conditions.* Ecological Engineering, 2016. **90**: p. 120-124.

14. Abdo, P. and B.P. Huynh, *An experimental investigation of green wall bio-filter towards air temperature and humidity variation.* Journal of Building Engineering, 2021. **39**: p. 102244.
15. Mangone, G., S.R. Kurvers, and P.G. Luscuere, *Constructing thermal comfort: Investigating the effect of vegetation on indoor thermal comfort through a four season thermal comfort quasi-experiment.* Building and Environment, 2014. **81**: p. 410-426.
16. Wetzel, T.A. and W.J. Doucette, *Plant leaves as indoor air passive samplers for volatile organic compounds (VOCs).* Chemosphere, 2015. **122**: p. 32-37.
17. Wild, E., et al., *Direct Observation of Organic Contaminant Uptake, Storage, and Metabolism within Plant Roots.* Environmental Science & Technology, 2005. **39**(10): p. 3695-3702.
18. Rodgers, K., R. Handy, and W. Hutzel, *Indoor air quality improvements using Biofiltration in a highly efficient residential home* Journal of Green Building, 2013. **8**(1): p. 22-27.
19. Zhang, L., R. Routsong, and S.E. Strand, *Greatly Enhanced Removal of Volatile Organic Carcinogens by a Genetically Modified Houseplant, Pothos Ivy (Epipremnum aureum) Expressing the Mammalian Cytochrome P450 2e1 Gene.* Environmental Science & Technology, 2019. **53**(1): p. 325-331.
20. Wolverton, B.C., R.C. McDonald, and E.A. Watkins, *Foliage plants for removing indoor air pollutants from energy-efficient homes.* Economic Botany, 1984. **38**(2): p. 224-228.
21. Lohr, V.I., C.H. Pearson-Mims, and G.K. Goodwin., *Interior plants may improve worker productivity and reduce stress in a windowless environment.* Journal of Environmental Horticulture 1996. **14**(2): p. 97-100.
22. Kim, J., et al., *The effects of indoor plants and artificial windows in an underground environment.* Building and Environment, 2018. **138**: p. 53-62.
23. Azkorra, Z., et al., *Evaluation of green walls as a passive acoustic insulation system for buildings.* Applied Acoustics, 2015. **89**: p. 46-56.
24. Hellinga, H. and G. de Bruin-Hordijk, *Assessment of daylight and view quality: a field study in office buildings.* International Commission on Illumination (Vienna, Austria: 2010), 2010: p. 326-31.
25. Lee, S., *Why Indoor Plants Make You Feel Better*, 2017, NBC news.
26. Hall, C. and M. Knuth, *An Update of the Literature Supporting the Well-Being Benefits of Plants: A Review of the Emotional and Mental Health Benefits of Plants.* Journal of Environmental Horticulture, 2019. **37**(1): p. 30-38.
27. Tove, F., *The Effect of Interior Planting on Health and Discomfort among Workers and School Children.* HortTechnology, 2000. **10**(1): p. 46-52.
28. Lohr, V.I. and C.H. Pearson-Mims, *Physical Discomfort May Be Reduced in the Presence of Interior Plants.* HortTechnology, 2000. **10**(1): p. 53-58.
29. Wang, L., E. Iddio, and B. Ewers, *Introductory overview: Evapotranspiration (ET) models for controlled environment agriculture (CEA).* Computers and Electronics in Agriculture, 2021. **190**: p. 106447.
30. Brümmer, C., et al., *How climate and vegetation type influence evapotranspiration and water use efficiency in Canadian forest, peatland and grassland ecosystems.* Agricultural and Forest Meteorology, 2012. **153**: p. 14-30.

31. Qiu, R., et al., *Response of evapotranspiration and yield to planting density of solar greenhouse grown tomato in northwest China.* Agricultural Water Management, 2013. **130**: p. 44-51.
32. Allen, R., *Penman-Monteith Equation*, in *Encyclopedia of Soils in the Environment*, D. Hillel, Editor 2005, Elsevier: Oxford. p. 180-188.
33. Graamans, L., et al., *Plant factories; crop transpiration and energy balance.* Agricultural Systems, 2017. **153**: p. 138-147.
34. Stanghellini, C., *Transpiration of Greenhouse Crops – an Aid to Climate Management*, 1987, Institute of Agricultural Engineering.
35. Fynn, R.P., et al., *Evapotranspiration measurement and modeling for a potted chrysanthemum crop.* American Society of Agriculture Engineers, 1993. **36**(6): p. 1907-1913.
36. Takakura, T., et al., *Measurement of evapotranspiration rate in a single-span greenhouse using the energy-balance equation.* Biosystems Engineering, 2009. **102**(3): p. 298-304.
37. Allen, R.G., et al., *Crop evapotranspiration-Guidelines for computing crop water requirements*, 1998: Rome, Italy.
38. Hargreaves, G. and Z. Samani, *Reference crop evapotranspiration from temperature.* Applied Engineering in Agriculture, 1985. **1**(2): p. 96–99.
39. Baille, M., A. Baille, and J.C. Laury, *A simplified model for predicting evapotranspiration rate of nine ornamental species vs. climate factors and leaf area.* Scientia Horticulturae, 1994. **59**(3): p. 217-232.
40. Bailey, B.J., et al., *Transpiration of Ficus benjamina: comparison of measurements with predictions of the Penman-Monteith model and a simplified version.* Agricultural and Forest Meteorology, 1993. **65**(3): p. 229-243.
41. Priestley, C.H.B. and R.J. Taylor, *On the Assessment of Surface Heat Flux and Evaporation Using Large-Scale Parameters.* Monthly Weather Review, 1972. **100**(2): p. 81-92.
42. WMO, *Measurement and estimation of evaporation and evapotranspiration*, 1966, World Meteorological Organization: Geneva, Switzerland.
43. Blaney, H. and W. Criddle, *Determining water requerrimients in irrigation area from climatological and irrigation data.* Washington DC: USDA, 1950.
44. Shuttleworth, W.J., *Evaporation* in *Handbook of Hydrology* D.R. Maidment, Editor 1993, New York: McGraw-Hill
45. Guo, D. and S. Westra, *Evapotranspiration: modeling actual, potential and reference crop evapotranspiration. R package version 1.10*, 2016.
46. Morton, F.I., *Operational estimates of areal evapotranspiration and their significance to the science and practice of hydrology.* Journal of Hydrology, 1983. **66**(1): p. 1-76.
47. Hobbins, M.T., J.A. Ramírez, and T.C. Brown, *The complementary relationship in estimation of regional evapotranspiration: An enhanced advection-aridity model.* Water Resources Research, 2001. **37**(5): p. 1389-1403.
48. Malys, L., M. Musy, and C. Inard, *A hydrothermal model to assess the impact of green walls on urban microclimate and building energy consumption.* Building and Environment, 2014. **73**: p. 187-197.
49. van de Wouw, P.M.F., E.J.M. Ros, and H.J.H. Brouwers, *Precipitation collection and evapo(transpi)ration of living wall systems: A comparative study between a panel system and a planter box system.* Building and Environment, 2017. **126**: p. 221-237.

50. He, Y., et al., *An investigation on the thermal and energy performance of living wall system in Shanghai area.* Energy and Buildings, 2017. **140**: p. 324-335.
51. Allen, R.G., et al., *Crop evapotranspiration-Guidelines for computing crop water requirements-FAO Irrigation and drainage paper 56.* Fao, Rome, 1998. **300**(9): p. D05109.
52. DOE. *EnergyPlus Energy Simulation Software, Version 9.6.* . 2021; Available from: https://github.com/NREL/EnergyPlus/releases/tag/v9.6.0.
53. DOE. *Commerical Reference Buildings*. Available from: http://energy.gov/eere/buildings/commercial-reference-buildings.
54. LI-COR, *Using the LI-6400/LI-6400XT portable photosynthesis system (Version 6)*, Lincoln, Nebraska: LI-COR Biosceinces, Inc.
55. Gimenez, C., M. Gallardo, and R.B. Thompson, *PLANT–WATER RELATIONS*, in *Encyclopedia of Soils in the Environment*, D. Hillel, Editor 2005, Elsevier: Oxford. p. 231-238.
56. Jarvis, P., *The interpretation of the variations in leaf water potential and stomatal conductance found in canopies in the field.* Phil. Trans. R. Soc. Lond. B, 1976. **273**(927): p. 593-610.
57. Ball, J.T., I.E. Woodrow, and J.A. Berry, *A model predicting stomatal conductance and its contribution to the control of photosynthesis under different environmental conditions*, in *Progress in photosynthesis research* 1987, Springer. p. 221-224.
58. Li, K., et al., *Identification of typical building daily electricity usage profiles using Gaussian mixture model-based clustering and hierarchical clustering.* Applied Energy, 2018. **231**: p. 331-342.
59. Wang, L., R. Kubichek, and X. Zhou, *Adaptive learning based data-driven models for predicting hourly building energy use.* Energy and Buildings, 2018. **159**: p. 454-461.
60. Shimizu, N. and H. Kaneko, *Direct inverse analysis based on Gaussian mixture regression for multiple objective variables in material design.* Materials & Design, 2020. **196**: p. 109168.
61. El Zaatari, S., W. Li, and Z. Usman, *Ring Gaussian Mixture Modelling and Regression for collaborative robots.* Robotics and Autonomous Systems, 2021. **145**: p. 103864.
62. Fraley, C. and A.E. Raftery, *Bayesian Regularization for Normal Mixture Estimation and Model-Based Clustering.* Journal of Classification, 2007. **24**(2): p. 155-181.
63. Bishop, M., *Pattern Recognition and Machine Learning.* 2006: Springer.
64. Sung, H.G., *Gaussian mixture regression and classification*, in *Statistics* 2004, Rice University: Houston, Texas.
65. ASHRAE, *ASHRAE Guideline 14: Measurement of Energy, Demand and Water Savings*, 2014, American Society of Heating, Refrigeration and Air Conditioning Engineers: Atlanta, GA.
66. ASHRAE, *ANSI/ASHRAE Standard 62.1-2019, Ventilation for Acceptable Indoor Air Quality*, 2019, American Society of Heating, Refrigerating and Air-Conditioning Engineers: Atlanta,GA.